Analytical and FE Modeling for the Design of Coreless Axial Flux Machines with Halbach Array and Surface PM Rotors

Matin Vatani
SPARK Lab, Pigman Eng. College
University of Kentucky
Lexington, KY, USA
matin.vatani@uky.edu

Yaser Chulaee
SPARK Lab, Pigman Eng. College
University of Kentucky
Lexington, KY, USA
yaser.chulaee@uky.edu

John F. Eastham
Dept. of Electronic & Electrical Eng.
University of Bath
Claverton Down, Bath, UK
jfeastham@aol.com

Dan M. Ionel
SPARK Lab, Pigman Eng. College
University of Kentucky
Lexington, KY, USA
dan.ionel@ieee.org

***Abstract*—This paper introduces a rapid analytical modeling approach for coreless axial flux permanent magnet (AFPM) machines featuring surface-mounted and Halbach PM array rotors. The methodology employs a 2D model at an arbitrary diameter of the machine and converts AFPM machines into an equivalent linear machine. Initially, equations for PM flux density, accounting for harmonic content, are developed for both rotor types. Subsequently, a force equation is derived for the 2D equivalent machine based on the Lorentz force equation and the stator winding factor. In the final step, a torque equation at an arbitrary diameter—specifically, the average diameter in this paper—is formulated using matching boundary conditions. The developed analytical model is validated through 2D/3D finite element analysis (FEA) and experimental measurements. This analytical framework is then applied to conduct a parametric study, aiming to assess the impact of Halbach array PM rotor dimensions on the performance of a coreless AFPM machine for electric aircraft propulsion. The results of this study provide a sizing methodology for Halbach array rotors, enabling the achievement of maximum specific power density and efficiency in coreless stator AFPM machines.**

***Index Terms*—Axial flux PM machines, analytical, coreless AFPM, electric aircraft, Halbach array, 2/3D FEA.**

I. Introduction

Aircraft electrification is being explored to reduce fuel consumption, emissions, and noise and to meet the growing demand for air travel. For both fully electric and hybrid aircraft, it is crucial to minimize the weight of electric motors and their related components, such as power electronics and cooling systems. This requires a multiphysics design optimization approach at both the component and system levels, as highlighted by Rosu *et al.* [1].

Among different electric machine topologies and types, Aydin *et al.* [2] and Nishanth *et al.* [3] has shown that axial flux permanent magnet (AFPM) machines offer higher specific power compared to their radial counterparts. Additionally, Gieras *et al.* [4] demonstrated that further enhancements in specific power density for AFPM machines may be achieved by removing the stator core.

Aydin *et al.* [2] discussed that coreless stator AFPM machines can be more efficient than conventional machines due to the elimination of core-associated losses. Chulaee *et al.* [5] demonstrated that using a Halbach array rotor significantly enhances the torque capability of a coreless AFPM machine compared to a conventional surface-mounted PM rotor under the same electrical loading. Vatani *et al.* [6] discussed the geometric proportions of a Halbach array for maximum power density in a naturally cooled, large airgap coreless AFPM generator. They noted that a larger magnet-to-magnet (M2M) gap could be offset by increasing the number of turns in the airgap, although this comes at the expense of efficiency.

Axial flux machines are complex 3D electromagnetic problems due to radial flux variations and fringing effects at both outer and inner radii, as noted by [7]. In coreless stator AFPM machines, these issues are exacerbated by the larger airgap and absence of the stator core. Accurate modeling necessitates 3D calculations, but 3D finite element analysis (FEA) is computationally intensive and time-consuming for large multiphysics design optimization.

A 2D approach for modeling AFPMs was proposed by Eastham *et al.* [8]. This method involves cutting the machine at the average radius to produce a cylindrical surface, which is then unrolled to create an equivalent 2D model. This paper employs Eastham's method to calculate flux density and to develop the torque equation for coreless AFPM machines.

II. Coreless Stator AFPM Machine Topologies

The topology of the coreless stator AFPM machines under investigation is illustrated in Fig. 1. These machines have two external rotor structures, which can feature surface-mounted

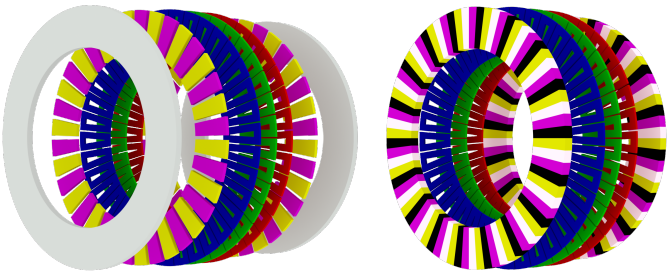

(a) (b)

Fig. 1. Exploded view of the coreless AFPM machines under study, with (a) surface PM and (b) Halbach rotors.

or Halbach array rotors. Between these rotors lies a coreless stator with overlapping windings.

For the surface-mounted rotor configuration, the axially magnetized PMs are fixed to a back iron disk, which acts as the flux return path. In contrast, the Halbach array rotor configuration directs the magnetic flux through tangentially magnetized PMs, eliminating the need for a back iron.

The geometric dimensions and ratings of the machines under investigation are derived from a coreless AFPM machine prototype, depicted in Fig. 2. The design specification of the prototyped machine has been presented by Chulaee *et al.* [5], featuring a double-sided surface-mounted rotor and a coreless printed circuit board (PCB) stator. The stator, characterized by overlapping windings, is comprised of three distinct PCBs, each corresponding to one phase. Detailed geometric dimensions and ratings are listed in Table I.

The exact dimensions, including the rotor's outer and inner diameters and the number of poles, were used for the machine with the Halbach PM array rotor. To ensure a fair comparison between the surface-mounted PM and Halbach array machines, beyond merely developing their analytical models, the axial length of both rotors was kept identical. This means that the PM length in the Halbach array rotor machine is equivalent to the combined lengths of the PM and back iron in the surface-mounted PM machine.

III. Magnetic Field Analysis

A. Analytical and FEA Flux Density Analysis

For a double-sided surface-mounted PM linear rotor, depicted in Fig. 3a, the normal and tangential airgap flux density distributions are [9–11]:

$$B_x = \sum_{i=0}^{\infty} B_{n_{SPM}} \sinh\left(\frac{n\pi y}{\tau_p}\right) \sin\left(\frac{n\pi\,(2x+\tau_p)}{2\tau_p}\right); \quad (1)$$

$$B_y = \sum_{i=0}^{\infty} B_{n_{SPM}} \cosh\left(\frac{n\pi y}{\tau_p}\right) \cos\left(\frac{n\pi\,(2x-\tau_p)}{2\tau_p}\right), \quad (2)$$

where $n = 1 + 2i$ and τ_p is the pole pitch at average diameter. The pole pitch can be calculated using $\tau_p = \frac{\pi D_{avg}}{p}$, where D_{avg} is the average diameter and p is the pole number. $B_{n_{SPM}}$

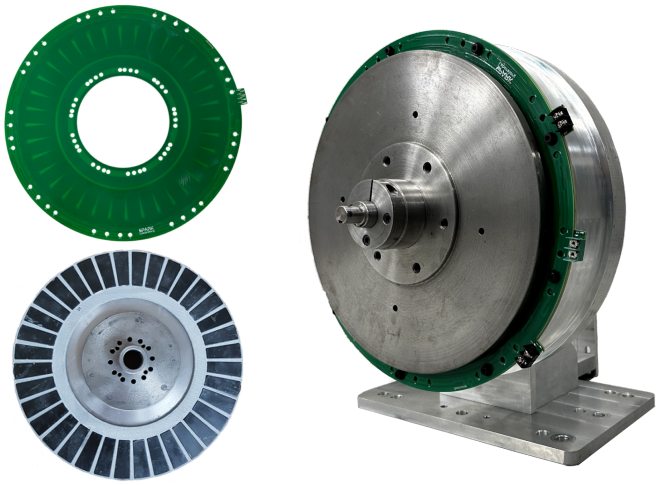

(a) (b)

Fig. 2. Coreless PCB stator AFPM machine with surface-mounted PM rotor, rated at 19 N·m and 2,100 rpm, used for analytical modeling verification.

Table I
Specifications and main dimensions of the prototyped coreless AFPM with surface PM rotor.

Parameter	Description	Value
OD	Outer diameter [mm]	304
P	Pole number [-]	36
Kg_{M2M}	PM-to-PM gap [mm]	8.6
$L_{PM_{Hal}}$	Halbach rotor PM length [mm]	11.0
$L_{PM_{SPM}}$	SPM rotor PM length [mm]	4.8
$K_{rl} = (OD_r - ID_r)/OD_r$	Radial length ratio [-]	0.32
$K_{w_{SPM}} = w_{PM/\tau_p}$	PM width to pole pitch ratio [-]	0.8
l_g	Mechanical airgap [mm]	1.3
P_{out}	Output power [kW]	4.18
n	Speed [rpm]	2,100

can be obtained from:

$$B_{n_{SPM}} = 4B_r \cdot \frac{\sin\left(n\pi w_{PM}/2\tau_p\right)}{n\pi} \cdot \frac{\sinh\left(n\pi L_{PM}/\tau_p\right)}{\sinh\left(n\pi(L_{PM}+g_{M2M}/2)/\tau_p\right)}, \quad (3)$$

where B_r is the remanence of the PMs, w_{PM} is the PM width, L_{PM} is the PM length, and g_{M2M} is the magnet-to-magnet gap distance.

The initial 2D analytical calculation of flux density for a double-sided linear Halbach PM array was first developed by Mallinson [12] and Halbach [13], with an enhanced version later presented by Ramian *et al.* [14]. Their method involved solving Poisson's equations and employing Fourier transforms. The normal and tangential components of flux density for a double-sided Halbach array, Fig. 3b, can be determined as:

$$B_x = \sum_{i=0}^{\infty} B_{n_{Hal}} \sinh\left(\frac{n\pi y}{\tau_p}\right) \cos\left(\frac{n\pi x}{\tau_p}\right); \quad (4)$$

$$B_y = \sum_{i=0}^{\infty} B_{n_{Hal}} \cosh\left(\frac{n\pi y}{\tau_p}\right) \sin\left(\frac{n\pi x}{\tau_p}\right), \quad (5)$$

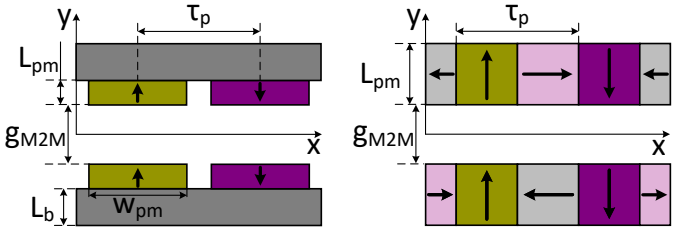

Fig. 3. Rotor geometrical parameters for (a) SPM and (b) Halbach array, used for the analytical flux density calculation.

where $B_{n_{Hal}}$ can be calculated from:

$$B_{n_{Hal}} = 2B_r \cdot \frac{\sin(\epsilon n\pi/m)}{n\pi/m} \cdot \left[1 - \exp\left(\frac{-n\pi L_{PM}}{\tau_p}\right)\right] \exp\left(\frac{-n\pi g_{M2M}}{2\tau_p}\right) \quad (6)$$

where is ϵ usually set to one, $n = 1 + mi$, and m is the number of PMs per wavelength.

The normal component of flux density for the motors described in Section II was calculated using the presented analytical and 2D FEA modeling, with the results shown in Fig. 3a. The analytical calculations closely align with the 2D FEA results. These calculations were performed at the midpoint of the airgap, i.e., $y = 0$, where the flux density harmonics are minimal. However, calculations at different y positions yield results with similar accuracy.

Compared to the conventional rotor, as shown in Fig. 4a, the Halbach array variant achieves roughly 30% higher flux density within the same envelope and exhibits lower harmonic content. This potentially allows a machine with a Halbach rotor to generate more power than a similarly sized machine with a surface-mounted rotor. However, this improvement comes at a significantly higher cost due to the increased amount of PM material required for the Halbach array.

The tangential component of airgap flux density for both rotor variants was calculated using analytical and 2D FEA methods, with the results shown in Fig. 4b. At $y = 0$, the tangential flux density component is zero for both rotor configurations due to their double-sided structure. The figure presents the calculations at the stator surface, corresponding to $y = -3$ mm. The analytical formulas accurately capture the significant harmonic content of the tangential flux. Evaluating the tangential flux density component is crucial for assessing the normal forces between the stator and rotors and determining the conductors' eddy current losses.

The flux densities calculated using 2D methods can accurately determine flux density values at a specific radius and slice of the machine. Although these calculations do not account for the curvature effects present in AFPM machines, performing 2D calculations at different radii shows only a slight deviation from those calculated at the average radius for the machine under study. This eliminates the need to evaluate flux density at multiple radii.

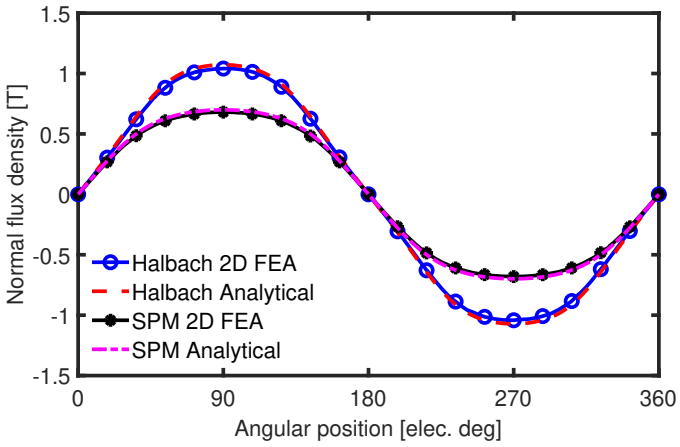

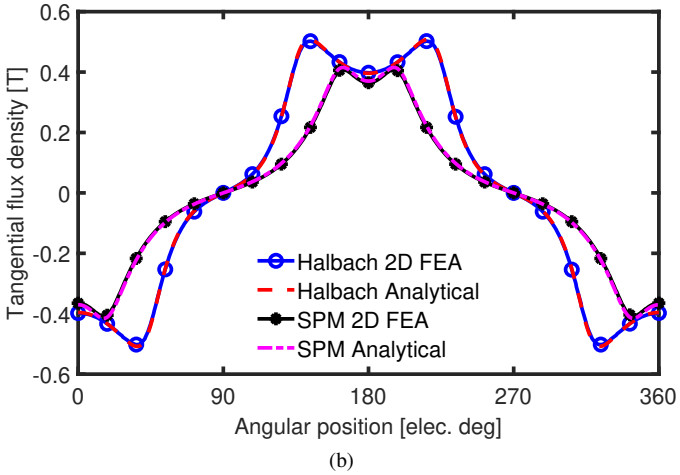

Fig. 4. Normal component of flux density calculated at the midpoint of the airgap ($y = 0$) (a) and tangential component calculated at the stator surface ($y = -3$ mm) (b).

This may not hold true for AFPM machines with larger outer diameters and extensive radial lengths. In such cases, the necessary 3D modeling of AFPM machines can be simplified by using multiple 2D equivalent models at different radii. The overall performance can then be determined by superimposing the results of all slices. Examples of multi-slice 2D calculations for AFPM machines have been presented by Gulec *et al.* [15] and Kim *et al.* [16].

The 2D modeling of AFPM machines does not account for the edge effects at the outer and inner radii. The fringing flux is more significant in coreless stator AFPM machines, where the electromagnetic airgap is relatively larger than in conventional AFPM machines. The 3D flux density distribution for the coreless AFPM machines under study is shown in Fig. 5 for a 360 electrical degree span, highlighting the fringing flux at the outer diameter.

At the outer and inner radii, where the fringing flux is present, 2D methods cannot accurately evaluate the flux density. This fringing flux can contribute to torque production if the stator has a larger outer diameter than the rotor. The edge effect can be partially accounted for in 2D modeling by applying corrective coefficients. For example, Bumby *et*

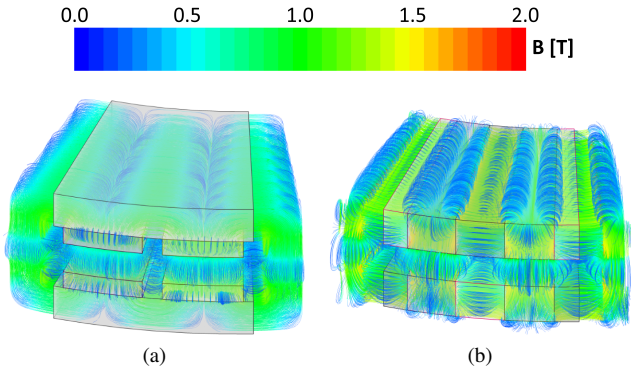

Fig. 5. No-load flux density distribution calculated using 3D FEA for (a) surface-mounted PM rotor and (b) Halbach PM array rotor.

al. [17] introduced a coefficient to compensate for significant fringing flux in an AFPM slot less stator machine, thereby incorporating the edge effect into the equivalent 2D model.

B. Effect of Permanent Magnet Numbers in Halbach Array

The Halbach array can be implemented with four PMs for each 360 electrical degrees, known as a 90-degree Halbach array, or scaled by a factor of four. The analytical equations developed account for the effect of the number of PMs, revealing that a higher number of PMs results in lower harmonic content amplitudes. This is important because harmonic content in PM flux density induces eddy currents in the conductors, reducing efficiency.

Two-dimensional FEA models at the average diameter were developed for Halbach array rotors with four, eight, and twelve PMs per wavelength, all of the same size. The flux density distribution at the middle of the airgap, calculated using both analytical and FEA methods, is presented in Fig. 6. The results indicate an approximately 11% improvement in the maximum flux density value for four PMs compared to eight. Increasing the number of PMs from eight to twelve does not further enhance the maximum flux density value.

The flux density harmonic spectrum for these three Halbach array rotor variants, calculated using 2D FEA, is shown in Fig. 7. The fundamental components were omitted, focusing on the harmonic content at the average diameter and middle of the airgap. For four PMs per wavelength, the expected harmonics are fourth order, eighth order for eight PMs, and twelfth order for twelve PMs. The results show a significant decrease in harmonic content for the eight and twelve PM Halbach arrays compared to the four PM variant.

IV. Winding Factor

The winding schematic of the prototyped coreless AFPM is illustrated in Fig. 8. This design incorporates a three-layer winding, where each layer has a thickness of 2 mm, though the figure exaggerates this for clarity. Each layer represents a distinct phase, with a 120-degree electrical shift between them. All layers are identical and contain the number of coils equal to the number of poles.

The winding factor is determined by multiplying the coil pitch and distribution factors. Detailed calculations for the

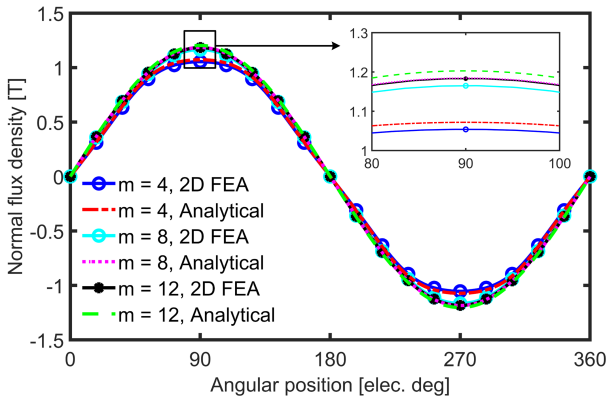

Fig. 6. Normal component of the flux density at the midpoint of the airgap for Halbach arrays with 4, 8, and 12 PMs per wavelength.

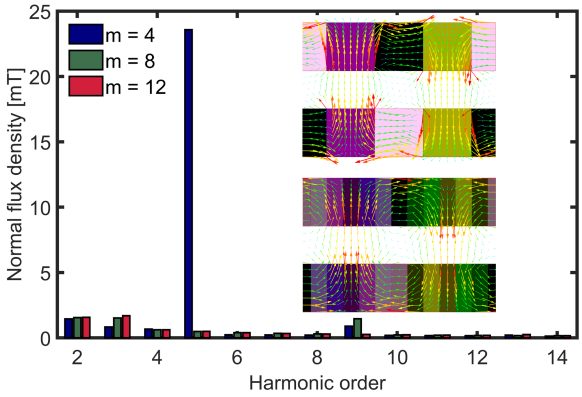

Fig. 7. Harmonic content of the normal component of the flux density at the midpoint of the airgap, excluding the fundamental component, for Halbach arrays with 4, 8, and 12 PMs per wavelength.

winding factor in various winding configurations of coreless linear PM and AFPM machines are provided by Eastham *et al.* [18] and Min *et al.* [19]. The winding pitch factor can be computed from:

$$k_p = \sin\left(\frac{n\pi\tau_c}{2\tau_p}\right), \tag{7}$$

where $n = 1 + i$ denotes the harmonic order, with i beginning at zero. The coil pitch, τ_c, is calculated using the formula $\tau_c = \frac{\pi D_{avg}}{N_c} - w_{cs}$, where N_c is the number of coils in one circumferential period of the machine. The distribution factor in the x direction can be calculated as:

$$k_{dx} = \frac{N_c}{n\pi K}\sin\left(\frac{n\pi K}{N_c}\right), \tag{8}$$

where K is coil side width to coil width ratio $K = \frac{W_{cs}}{W_c}$.

V. Torque Calculations

In coreless PM machines, the generation of force or torque results from the interaction between the magnetic flux density (B) of the permanent magnets and the current density (J) in the conductors, known as the Lorentz force. As described by

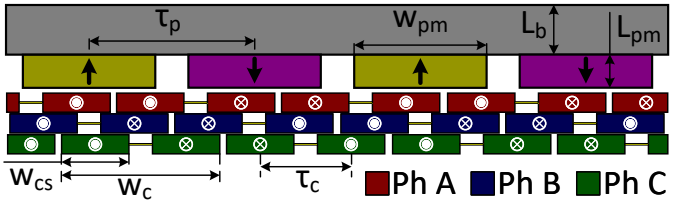

Fig. 8. Winding topology and geometrical parameters employed for winding factor calculation of the prototyped machine. The lower side rotor was not shown here to provide a better illustration.

Hayt *et al.* [20], the Lorentz equation is given by:

$$F = \int_v J \times B \, dv, \tag{9}$$

where B can be determined using equations (1) through (6), and J can be obtained as:

$$J = \frac{NIk_w}{h_c w_c}, \tag{10}$$

where N is the number of turns per coil, I is the current, and $k_w = k_p k_{dx}$ is total winding factor.

By substituting the summation of tangential and normal components of flux density and (10) into equation (9), the integral simplifies into two terms: normal and tangential components. The normal force, which is the forces between stator and rotor, is crucial in the mechanical design of coreless stator PM machines, while the tangential component generates the propulsive force.

The tangential force component can be derived by solving equation (9) for conductors carrying current in the z-direction and normal flux density components as:

$$F(x,i) = NLI_p \sum_{j=1}^{3} \sum_{i=0}^{\infty} k_w B_n \sin\left(\frac{n\pi x}{\tau_p} + (1-j)\frac{4n\pi}{3}\right) \sin\left(\frac{\pi x}{\tau_p} + (1-j)\frac{4\pi}{3}\right), \tag{11}$$

where I_p represents the peak value of the phase current. $L = \frac{OD_r - ID_r}{2}$ is the rotor radial length, with OD_r and ID_r being the rotor's outer and inner diameters, respectively. j denotes the number of phases, and B_n is the flux density amplitude. For conventional SPM and Halbach rotors, B_n can be derived from equations (3) and (6), respectively.

To derive the torque equation for the coreless stator AFPM machine under study, (11) must be multiplied by P due to the symmetry boundary condition and by the average rotor radius, resulting in:

$$T = k_1 pNI_p \left(OD_r^2 - ID_r^2\right) \sum_{j=1}^{3} \sum_{i=0}^{\infty} k_w B_n \sin\left(\frac{n\pi x}{\tau_p} + (1-j)\frac{4n\pi}{3}\right) \sin\left(\frac{\pi x}{\tau_p} + (1-j)\frac{4\pi}{3}\right), \tag{12}$$

where k_1 depends on the number coils and poles and their resultant matching boundary condition. For the prototyped machine with the described winding pattern, $k_1 = \frac{1}{4}$. In (12), the radius dependent parameters, including τ_p, τ_c, and position, x, are calculated at the average rotor diameter, $(OD_r + ID_r)/2$.

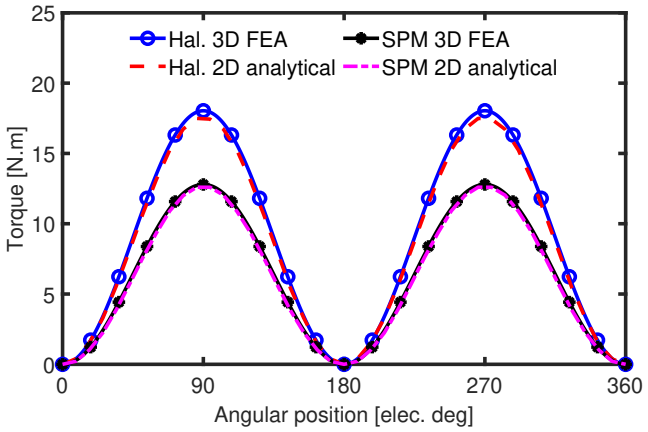

Fig. 9. Comparison of the single-phase torque for the prototyped coreless AFPM machine, analytically calculated and simulated using a 3D FEA tool for Phase B which is positioned between the other two phases in the airgap.

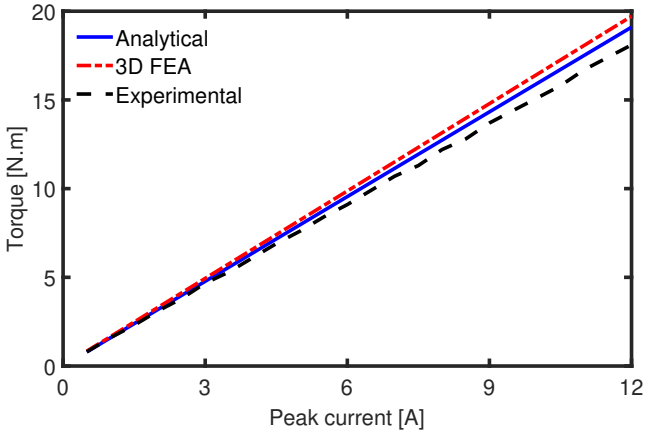

Fig. 10. Three-phase torque across different DC current values, comparing analytical calculations, 3D FEA simulations, and experimental measurements. The measurements was performed at discrete DC current values.

To validate the developed analytical model, the coreless AFPM machines were modeled using 3D FEA. The single-phase torque calculated by both methods is compared and presented in Fig. 9, demonstrating a strong agreement between the results. Additionally, the figure shows that a Halbach array rotor generates approximately 40% more torque compared to the surface PM rotor within the same rotor envelope.

The three-phase torque at various phase current levels was experimentally measured and compared with calculations from 3D FEA and analytical models for the coreless AFPM machine prototype with a surface-mounted PM rotor. The results, shown in Fig. 10, indicate a close agreement between the methods. It is important to note that the developed analytical calculations do not account for back iron saturation and are only valid when the back iron is sufficiently thick to prevent saturation, as is the case with the prototype machine.

VI. Halbach Array Rotor Design Considerations and Discussion for Electric Aircraft Propulsion

In this section, the analytically developed and numerically and experimentally validated model is used to investigate the

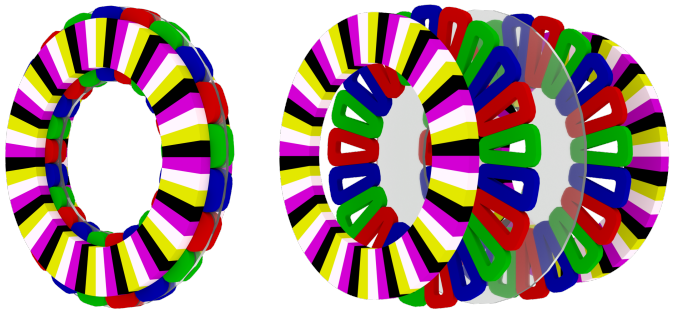

(a) (b)

Fig. 11. Coreless AFPM machine designed for electric aircraft propulsion, rated at 1.5 MW and 3,000 rpm, with an outer diameter of 500 mm.

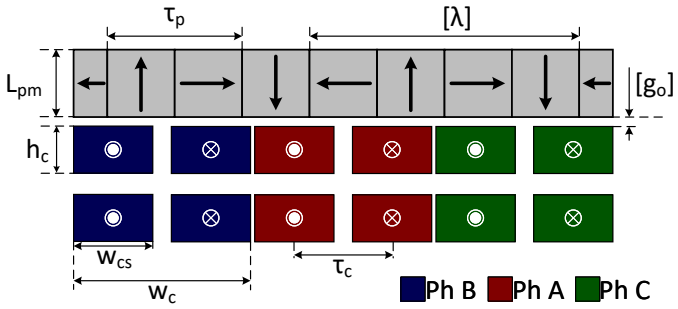

Fig. 12. Winding geometrical parameters used for calculating the winding factor. The lower side of the rotor is omitted for clarity in the illustration.

impact of Halbach array geometric parameters on a coreless AFPM machine proposed for electric aircraft propulsion. The topology of the proposed machine by Vatani *et al.* [21] in both compact and exploded views, highlighting the electromagnetic components, is illustrated in Fig. 11.

The proposed coreless AFPM machine features a double-sided Halbach PM array rotor with four PMs per wavelength. The stator comprises two sets of three-phase windings with concentrated coils and a coil pitch of 240 electrical degrees. Each stator provides half of the total power and is connected to a separate inverter to enhance fault tolerance. An axial direct cooling system is incorporated between the two stators to support higher current density values. A cryogenic coolant circulates within the cooling pad to dissipate heat generated by the stator windings.

In order to adapt the analytical model developed for performance evaluation of the described coreless AFPM, various considerations are necessary. While the winding pitch factor, distribution factor in the x-direction, and flux density equations remain valid, an additional winding distribution factor in the y-direction must be included. This is because, in coreless AFPMs with a relatively large magnet-to-magnet gap, conductors further from the PM surface are exposed to lower flux density. For the stator shown in Fig. 12, the winding distribution factor in the y-direction can be calculated as:

$$k_{dy} = \frac{2\tau_p}{n\pi h_c} \tanh\left(\frac{n\pi h_c}{2\tau_p}\right). \tag{13}$$

Furthermore, the circumferential periodicity of this machine

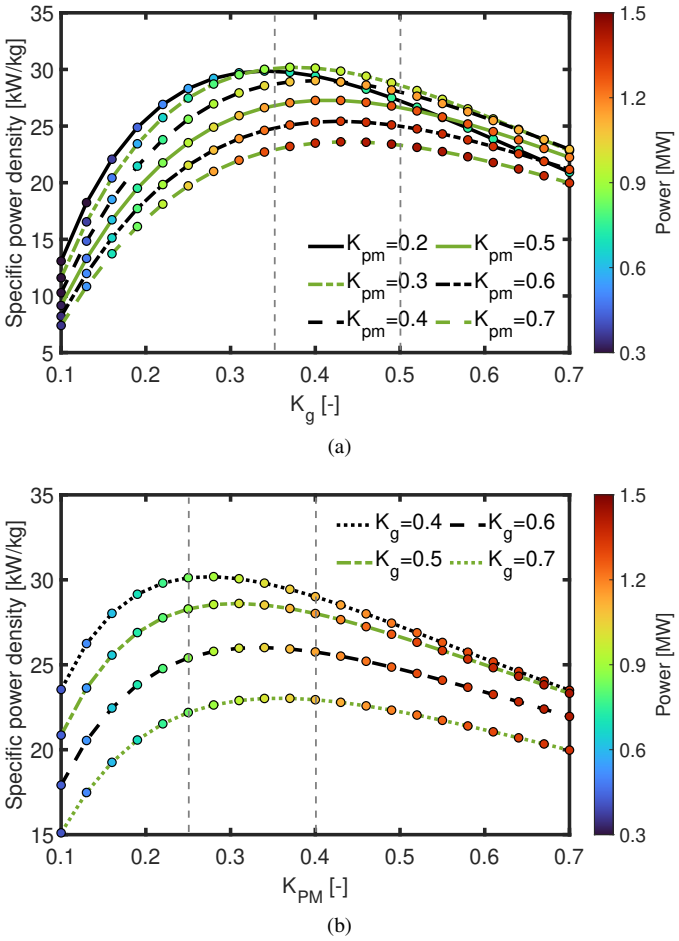

Fig. 13. Halbach array analytical parametric study results for variable (a) PM length and (b) M2M gap of an example coreless AFPM for electric aircraft. The ampere-turn was modified for each M2M gap accordingly.

differs from that of the prototyped machine analyzed in the previous section. The boundary condition can be applied for every $\frac{8\pi}{p}$, where p is the number of poles. Consequently, the factor k_1 must be adjusted to $k_1 = \frac{1}{16}$.

In equation (12), several parameters can be influenced by the geometry of a double-sided Halbach array, including the ampere-turn, rotor radial length, PM length, and magnet-to-magnet (M2M) gap. A parametric study for PM length and M2M gap using analytical equations was conducted to determine the optimal geometry of the Halbach array. These variables were varied from 0.1 to 0.7 times the pole pitch, $0.1 \leq \left(k_g = \frac{g_{M2M}}{\tau_p}\right)$ and $\left(k_{PM} = \frac{L_{PM}}{\tau_p}\right) \leq 0.7$. The ampere-turn was adjusted for each M2M gap based on the coil height, h_c, which was calculated from $h_c = K_g\tau_p - 2g_0 - l_{cool}$ where g_0 represents the mechanical airgap between the stator and rotor, l_{cool} is the axial cooling length between the stators.

The results of the parametric study for varying PM lengths are presented in Fig 13a. It shows that the optimal value for K_{PM} depends on the M2M gap: a thicker PM is preferred for larger gaps to counteract the drop in flux density. The highest specific power density is achieved for $0.25 \leq K_{PM} \leq 0.4$, depending on the M2M gap. Choosing K_{PM} outside this range may increase power output but at the expense of a significant

reduction in specific power density and inefficient use of PMs.

The results of varying the M2M gap at different PM lengths are shown in Fig. 13b. These results indicate that the optimal M2M gap is dependent on the PM length. The highest specific power density values are achieved for $0.35 \leq K_g \leq 0.5$. While a larger K_g allows for increased ampere-turns and improved power output, it also leads to greater use of copper material, which reduces the specific power density in kW/kg and increases copper losses.

VII. Conclusion

The equivalent 2D analytical modeling of the coreless AFPM machine proposed in this paper has been validated through comparisons with both 2D and 3D FEA results and experimental measurements, demonstrating satisfactory agreement. This method offers rapid and precise torque and flux density calculations, making it suitable for large-scale multiphysics design optimizations. The analytical model is able to accurately estimate the performance of coreless AFPM machines with relatively small magnet-to-magnet (M2M) gaps. For larger M2M gaps, achieving highly accurate results necessitates integrating over the axial length of the stator coils with an axial-dependent flux density.

The optimal geometry proportions for the Halbach arrays were determined through parametric studies employing the developed analytical model. Halbach arrays rotors are increasingly utilized in electric motor designs for electric aircraft due to their high specific power capability. The analytical study indicated that to achieve the highest specific power with a Halbach array rotor, the PM axial length should be between 0.25 and 0.4 times the pole pitch, depending on the M2M gap size. Additionally, the highest specific power was achieved when the M2M gap was between 0.35 and 0.5 times the pole pitch, depending on the PM length.

Acknowledgment

This paper is based upon work supported by the National Aeronautics and Space Administration (NASA) through the University Leadership Initiative (ULI) #80NSSC22M0068. Any findings and conclusions expressed herein are those of the authors and do not necessarily reflect the views of NASA. The support of ANSYS Inc. and of University of Kentucky, the L. Stanley Pigman Chair in Power endowment is also gratefully acknowledged.

References

[1] M. Rosu, P. Zhou, D. Lin, D. M. Ionel, M. Popescu, F. Blaabjerg, V. Rallabandi, and D. Staton, *Multiphysics simulation by design for electrical machines, power electronics and drives*. John Wiley & Sons, 2017.

[2] M. Aydin, S. Huang, and T. A. Lipo, "Axial flux permanent magnet disc machines: A review," in *Conf. Record of SPEEDAM*, vol. 8, 2004, pp. 61–71.

[3] F. Nishanth, J. Van Verdeghem, and E. L. Severson, "A review of axial flux permanent magnet machine technology," *IEEE Transactions on Industry Applications*, 2023.

[4] J. F. Gieras, R.-J. Wang, and M. J. Kamper, *Axial flux permanent magnet brushless machines*. Springer Science & Business Media, 2008.

[5] Y. Chulaee, D. Lewis, M. Vatani, J. F. Eastham, and D. M. Ionel, "Torque and power capabilities of coreless axial flux machines with surface pms and Halbach array rotors," in *2023 IEEE International Electric Machines & Drives Conference (IEMDC)*. IEEE, 2023, pp. 1–6.

[6] M. Vatani, A. Mohammadi, D. Lewis, J. F. Eastham, and D. M. Ionel, "Coreless axial flux Halbach array permanent magnet generator concept for direct-drive wind turbine," in *2023 12th International Conference on Renewable Energy Research and Applications (ICRERA)*. IEEE, 2023, pp. 612–617.

[7] F. Giulii Capponi, G. De Donato, and F. Caricchi, "Recent advances in axial-flux permanent-magnet machine technology," *IEEE Transactions on Industry Applications*, vol. 48, no. 6, pp. 2190–2205, 2012.

[8] S. Gair, A. Canova, J. F. Eastham, and T. Betzer, "A new 2D FEM analysis of a disc machine with offset rotor," in *Proceedings of International Conference on Power Electronics, Drives and Energy Systems for Industrial Growth*, vol. 1. IEEE, 1996, pp. 617–621.

[9] N. Chayopitak and D. G. Taylor, "Performance assessment of air-core linear permanent-magnet synchronous motors," *IEEE transactions on magnetics*, vol. 44, no. 10, pp. 2310–2316, 2008.

[10] F. Marcolini, G. De Donato, F. G. Capponi, and F. Caricchi, "Design of a printed circuit board axial flux permanent magnet machine for high speed applications," *IEEE Transactions on Industry Applications*, vol. 60, no. 4, pp. 5919–5930, 2024.

[11] A. Mohammadpour, A. Gandhi, and L. Parsa, "Winding factor calculation for analysis of back emf waveform in air-core permanent magnet linear synchronous motors," *IET Electric Power Applications*, vol. 6, no. 5, pp. 253–259, 2012.

[12] J. Mallinson, "One-sided fluxes – a magnetic curiosity?" *IEEE Transactions on Magnetics*, vol. 9, no. 4, pp. 678–682, 1973.

[13] K. Halbach, "Physical and optical properties of rare earth Cobalt magnets," *Nuclear Instruments and Methods in Physics Research*, vol. 187, no. 1, pp. 109–117, 1981.

[14] G. Ramian, L. Elias, and I. Kimel, "Micro-undulator fels," *Nuclear Instruments and Methods in Physics Research Section A: Accelerators, Spectrometers, Detectors and Associated Equipment*, vol. 250, no. 1-2, pp. 125–133, 1986.

[15] M. Gulec and M. Aydin, "Implementation of different 2D finite element modelling approaches in axial flux permanent magnet disc machines," *IET Electric Power Applications*, vol. 12, no. 2, pp. 195–202, 2018.

[16] K.-H. Kim and D.-K. Woo, "Novel quasi-three-dimensional modeling of axial flux in-wheel motor with permanent magnet skew," *IEEE Access*, vol. 10, pp. 98 842–98 854, 2022.

[17] J. R. Bumby, R. Martin, M. Mueller, E. Spooner, N. Brown, and B. Chalmers, "Electromagnetic design of axial-flux permanent magnet machines," *IEE Proceedings-Electric Power Applications*, vol. 151, no. 2, pp. 151–160, 2004.

[18] S. P. Colyer, P. Arumugam, and J. F. Eastham, "Modular airgap windings for linear permanent magnet machines," *IET Electric Power Applications*, vol. 12, no. 7, pp. 953–961, 2018.

[19] S. G. Min and B. Sarlioglu, "3-d performance analysis and multiobjective optimization of coreless-type pm linear synchronous motors," *IEEE Transactions on Industrial Electronics*, vol. 65, no. 2, pp. 1855–1864, 2018.

[20] W. Hayt and J. Buck, *Engineering Electromagnetics*. McGraw-Hill Companies, Inc., 2012.

[21] M. Vatani, Y. Chulaee, A. Mohammadi, D. R. Stewart, J. F. Eastham, and D. M. Ionel, "On the optimal design of coreless AFPM machines with Halbach array rotors for electric aircraft propulsion," in *2024 IEEE Transportation Electrification Conference & Expo (ITEC)*. IEEE, 2024.